PAPER

Effect of Imperfect Channel Estimation on the Performance of Pilot Channel-Aided Coherent DS-CDMA System over Rayleigh-Fading Multipath Channel

Seokjun KO†, *Nonmember and* **Hyungjin CHOI**†, *Member*

SUMMARY This paper presents the bit-error rate (BER) performance of the RAKE receiver over a multipath Rayleigh fading channel. The closed-form BER in the downlink single-cell environment is obtained through the analysis of the imperfect channel estimation. We compute the BER as a function of energy-to-noise ratio per bit including the effect of multiple access interference and multipath interference, with channel and system parameters: number of diversity channels $L = 1$, 3, 6, 12; Doppler frequency shift with $f_D T = 0.008333$, 0.0167, 0.025; residual carrier frequency offset $\Delta f = -600 \sim 600\,\mathrm{Hz}$; averaging length of the channel estimator $N_p = 128$–1536 chips. This analysis allows predicting the system's performance and helps to optimize the parameter setting for the channel estimation process. We show that even if the optimal system parameters are used, the BER performance results in a minimal 4dB degradation in comparison to the perfect channel estimation. Finally, the theoretical results are verified by using the Monte-Carlo computer simulations.

key words: *channel estimation, Rayleigh fading, coherent RAKE receiver, dissimilar multipath channel*

1. Introduction

It is well known that a coherent direct-sequence code division multiple access (DS-CDMA) system uses the RAKE receiver to achieve a diversity improvement on a frequency-selective fading channel and its BER performance has been analyzed in some literatures [1]–[8]. In [2]–[5], the BER performances of the selection combiner (SC) and the maximal ratio combiner (MRC) for the number of diversity channels have been analyzed. Recently, the performance of the equal gain combiner (EGC) was studied [6]. However, most BER performances have assumed the limiting cases of perfect synchronization (in timing and carrier phase) with received signals over multipath fading channel. Our analysis concentrates here on the effect of imperfect channel estimation that results from the maximum Doppler frequency in mobile channels, the carrier frequency offset due to uncertainty in a local oscillator, and additive white Gaussian noise (AWGN).

In this paper, a coherent DS-CDMA system in the downlink single-cell environment will be investigated. The channel estimation is carried out using a Pilot channel, which is transmitted simultaneously with a Traffic channel. This method is very closely related to the IS-95 CDMA concept. In the Maximum-Likelihood (ML) channel estimation, an averaging process is introduced in order to suppress the noise influence. In this process, the channel estimation error occurs inevitably. Recently, the influence of channel estimation in the multipath fading environment was studied [7],[8]. In [7], however, the averaging effect of the channel estimation was analyzed in an integral form. Also, the carrier frequency offset due to imperfect local oscillator was not considered. It seems that the exact BER performance of a MRC in a Rayleigh fading channel has not yet been analyzed. In this paper, we apply a formula from Appendix B of [1] to solve this problem.

The paper is organized as follows. In Sect. 2, the DS-CDMA system model is introduced. In Sect. 3, the channel estimation and the compensation processes are described. In Sect. 4, the first- and second-order statistics of the demodulated signal are presented, and the derived BER performance is presented. In Sect. 5, the numerical results and the computer simulations under various channel environments are evaluated. Finally, a brief conclusion is given in Sect. 6.

2. System Model

The system model for performance evaluation is shown in Fig. 1. The transmitted signal includes Traffic and Pilot channel signals. A pseudo-noise (PN) spread-spectrum signal is passed through a multipath fading channel, further corrupted by carrier frequency offset as well as additive white Gaussian noise (AWGN), and demodulated by a coherent RAKE receiver employing channel estimator for phase recovery. The (residual) carrier frequency offset is assumed to be within $\pm$ 600 Hz by the frequency locked loops. Therefore, the channel estimator must recover the residual carrier frequency offset and the channel phase simultaneously. The transmitter, channel, and receiver models are described in detail in later subsections.

Manuscript received April 10, 1999.
Manuscript revised July 25, 1999.

†The authors are with the Department of Electrical and Computer Engineering, Sung Kyun Kwan University, 300 Chunchun-dong, Jangan-gu, Suwon 440-746, Korea.

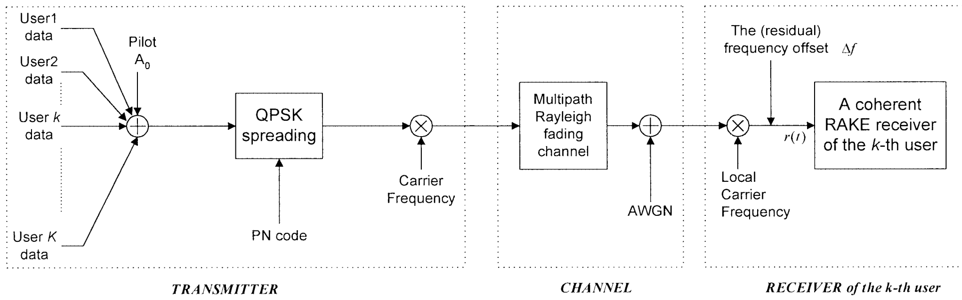

Fig. 1 DS spread spectrum communication system model with K users.

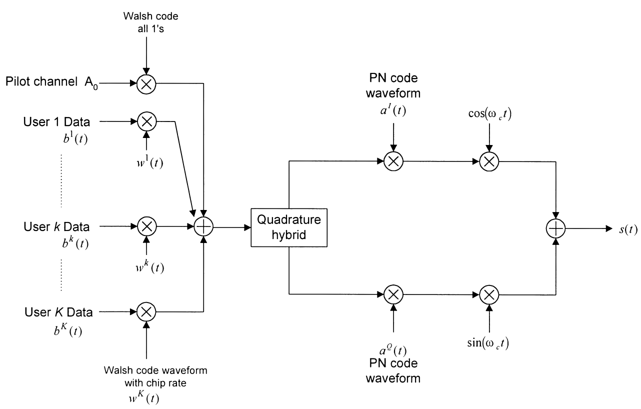

Fig. 2 Transmitter block diagram with K users.

2.1 Transmitter Model

The transmitter structure is shown in Fig. 2. A Walsh code sequence is used to distinguish between the Pilot channel (A_0) and the Traffic channel ($b(t)$) signals. The power at either output of the quadrature hybrid is one-half of the input power. The method of spreading modulation here is quadrature phase-shift keying (QPSK). This type of modulation is called balanced QPSK modulation since the data modulation is balanced between the in-phase and the quadrature-phase spreading channels [13]. Note, however, that data is essentially binary phase-shift keying (BPSK) modulated since the same data is applied to both I and Q channels.

The PN code sequence is assumed periodic with period (N_{PN}) much longer than the processing gain (N); the code sequence has a chip rate of $1/T_c$, where $T = NT_c$, and $1/T$ is the data bit rate. Let $a^I(t)$ and $a^Q(t)$ in Fig. 2 denote the in-phase and quadrature-phase PN code sequence waveforms, and let $\{a^I(t)\}$ and $\{a^Q(t)\}$ be the corresponding sequences of elements of $\{+1, -1\}$. Both spreading codes are assumed to be independent of each other. Then

$$\underline{a}(t) = a^I(t) - ja^Q(t), \quad \underline{a}(i) = a^I(i) - ja^Q(i),$$

where complex signals are underlined, $j = \sqrt{-1}$, and

$$a^I(t) = \sum_{i=-\infty}^{\infty} a^I(i) P_{T_c}(t - iT_c),$$

$$a^Q(t) = \sum_{i=-\infty}^{\infty} a^Q(i) P_{T_c}(t - iT_c),$$

where $P_{T_c}(t) = 1$ for $0 < \mathrm{t} < T_c$ and zero otherwise. Also, let $w(t)$ denote the Walsh code waveform, and let $w(i)$ be the corresponding sequence of elements of $\{+1, -1\}$. Then $w(t)$ is

$$w(t) = \sum_{i=-\infty}^{\infty} w(i) P_{T_c}(t - iT_c).$$

Similarly, the data signal waveform $b(t)$ can be written as

$$b(t) = \sum_{i=-\infty}^{\infty} b(i) P_T(t - iT).$$

The transmitted signal having K users is, therefore, given by

$$s(t) = \mathrm{Re}\left[\left\{\sqrt{E_c}A_o + \sum_{q=1}^{K} \sqrt{E_c^q} \cdot b^q(t) w^q(t)\right\} \times \underline{a}(t) e^{j\phi} e^{j\omega_c t}\right], \tag{1}$$

where $\sqrt{E_c}$ is the average transmitted power of the Pilot channel, $\sqrt{E_c^q}$ is the average transmitted power of each user, ω_c is the carrier frequency, and ϕ is the phase of the carrier. Without loss of generality, we may assume that ϕ is zero radians.

2.2 WSSUS Model for the Channel

The channel impulse response, $\underline{h}(\tau, t)$, is assumed to be a wide-sense stationary uncorrelated scattering (WSSUS) zero-mean white Gaussian process [10],[11]. For L resolvable paths, the impulse response of a frequency selective multipath radio channel can be represented by

$$\underline{h}(\tau, t) = \sum_{p=1}^{L} \alpha_p(t) e^{-j\phi_p(t)} \cdot \delta[\tau - \tau_p(t)], \tag{2}$$

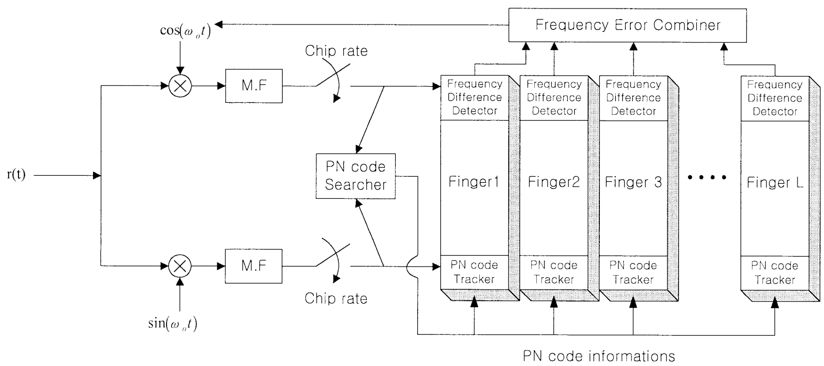

Fig. 3 Receiver block diagram of k-th user.

where $\alpha_p(t)$, $\phi_p(t)$, and $\tau_p(t)$ are the p-th path gain, phase, and delay, respectively. In this paper, we assume that the number of paths, L, may be either fixed. We assume, for each p, that $\alpha_p(t)$ is an independent Rayleigh distributed random (amplitude) variable, while the independent path delay $\tau_p(t)$, relative to the delay of a dominant path, is allowed to have any distribution in [0, T_c]. Further, we assume that the path phase $\theta_p(t)$, given by $(\omega_c\tau_p + \phi_p(t))$, is an independent random (phase) variable uniformly distributed in [0–2π). The parameter μ_p used in the Rayleigh distribution for $\alpha_p(t)$,

$$f_{\alpha_p}(x) = \begin{cases} \frac{x}{\mu_p}\exp\left(-\frac{x^2}{2\mu_p}\right) & x \geq 0 \\ 0 & x < 0 \end{cases}$$

is equal to half the average path power, i.e., $2\mu_p = E[(\alpha_p^I)^2] = E[(\alpha_p^Q)^2]$. In our model, μ_p may be different for each path and even be a function of $\tau_p(t)$.

2.3 Receiver Model

The receiver structure is shown in Fig. 3. This is a coherent RAKE receiver with L fingers (i.e., demodulators). The fingers are matched to the transmitted PN code and are assumed to have acquired time synchronization with each path of the signals.

With the input to the channel as given in (1), the output of the channel (which is also the input to the receiver) can be written as (in the sequel, only the complex envelope will be used)

$$\begin{aligned}\underline{r}(t) = &\frac{1}{2}\left\{\sum_{q=1}^{K}\sum_{p=1}^{L}\sqrt{E_c^q}\alpha_p(t)e^{j\phi_p(t)}b^q(t-\tau_p)\right.\\ &\left.\times\, w^q(t-\tau_p)\underline{a}(t-\tau_p)\cdot e^{j\omega_c(t-\tau_p)}e^{-j\omega_o t}\right\}\\ &+\left\{\frac{1}{2}\sum_{p=1}^{L}\sqrt{E_c}\alpha_p(t)e^{j\phi_p(t)}A_0\underline{a}(t-\tau_p)\right.\\ &\left.\times\, e^{j\omega_c(t-\tau_p)}e^{-j\omega_o t}\right\}+n(t)\end{aligned}$$

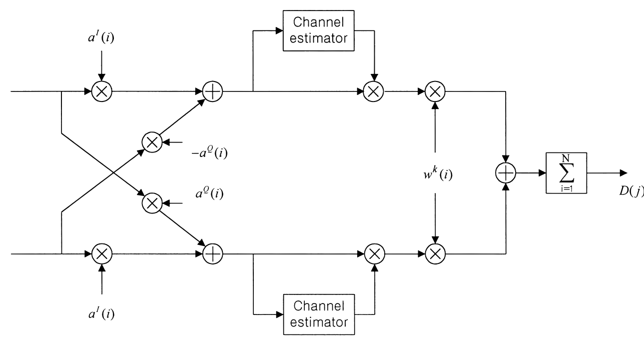

Fig. 4 Demodulator structure of k-th user for the l-th path.

$$\begin{aligned}&= \frac{1}{2}\left\{\sum_{q=1}^{K}\sum_{p=1}^{L}\sqrt{E_c^q}\alpha_p(t)e^{j\theta_p(t)}b^q(t-\tau_p)\right.\\ &\quad\left.\times w^q(t-\tau_p)\cdot\underline{a}(t-\tau_p)\ e^{j[2\pi\Delta f\cdot t]}\right\}\\ &\quad+\frac{1}{2}\left\{\sum_{p=1}^{L}\sqrt{E_c}\alpha_p(t)e^{j\theta_p(t)}A_0\underline{a}(t-\tau_p)\right.\\ &\quad\left.\times\ e^{j[2\pi\Delta f\cdot t]}\right\}+n(t) \qquad (3)\end{aligned}$$

where $2\pi\Delta f = \omega_c - \omega_o$ is carrier frequency offset and the carrier phase $\phi_p(t)$ has been absorbed in the random phase $\theta_p(t)$ associated with each channel path. The quantity denoted by $n(t)$ is the complex-valued lowpass-equivalent AWGN with noise spectral density $N_o/2$; therefore, $n(t)$ is a circularly symmetric, zero-mean Gaussian random process with covariance function $E[n(t)n^*(\tau)] = N_o\delta(t-\tau)$.

The demodulator structure for the l-th path is shown in Fig. 4. We assume that the spreading code's timing information of each path is estimated, i.e., for the p-th path τ_p is obtained through the synchronization process. So the received signals of all paths are exactly despread by the PN code searcher and tracker. The input signal to the fingers at optimal sampling instant may be separated into a signal component, denoted by U_S, and three noise components, denoted U_{MP}, U_{MAI} ,and U_N; the first noise component is due to "self-noise" from the multipath waveform of the signal, the second component is due to "multiple access interference" from the other users, and the third component is due to AWGN. Thus, the complex input signal of the k-th user's RAKE receiver is

$$\begin{aligned}\mathbf{U} &= [U_1, U_2, \cdots, U_l, \cdots, U_L]^T \\ &= \mathbf{U}_S + \mathbf{U}_{MP} + \mathbf{U}_{MAI} + \mathbf{U}_N\end{aligned} \tag{4}$$

where

$$\begin{aligned}&\mathbf{U}_S = [U_{S_1}, U_{S_2}, \cdots, U_{S_l}, \cdots, U_{S_L}]^T \\ &\mathbf{U}_{MP} = [U_{MP_1}, U_{MP_2}, \cdots, U_{MP_l}, \cdots, U_{MP_L}]^T \\ &\mathbf{U}_{MAI} = [U_{MAI_1}, U_{MAI_2}, \cdots, U_{MAI_l}, \cdots, U_{MAI_L}]^T \\ &\mathbf{U}_N = [U_{N_1}, U_{N_2}, \cdots, U_{N_l}, \cdots, U_{N_L}]^T\end{aligned}$$

where T indicates the transpose of the matrix.
From the channel and receiver models, the i-th sample value $U_{S_l}(i)$ of the k-th user for the l-th path can be represented as

$$\begin{aligned}U_{S_l}(i) &= \frac{\sqrt{E_c^k}}{2T_c} \int_{\tau_l}^{\tau_l+T_c} \Big\{ \alpha_l(\tau) e^{j[2\pi\Delta f(\tau)+\theta_l(\tau)]} \\ &\quad \times \left(A_o + b^k(\tau-\tau_l) w^k(\tau-\tau_l)\right) \\ &\quad \times \underline{a}(\tau-\tau_l) \Big\} d\tau \times \underline{a}^*(i) \\ &= \frac{\sqrt{E_c^k}}{2T_c} \alpha_l(i) e^{j[2\pi\Delta f\cdot i+\theta_l(i)]} \\ &\quad \times \int_0^{T_c} \left(A_o + b^k(t) w^k(t)\right) \underline{a}(t) dt \times \underline{a}^*(i) \\ &= \frac{\sqrt{E_c^k}}{2} \alpha_l(i) e^{j[2\pi\Delta f\cdot i+\theta_l(i)]} \\ &\quad \times \left(A_o + b^k(i) w^k(i)\right) \underline{a}(i) \times \underline{a}^*(i) \\ &= \sqrt{E_c^k} \alpha_l(i) e^{j[2\pi\Delta f\cdot i+\theta_l(i)]} \\ &\quad \times \left(A_o + b^k(i) w^k(i)\right)\end{aligned} \tag{5}$$

where $t = \tau - \tau_l$, τ_l is the path delay of the l-th multipath signal, and $\underline{a}(i) \times \underline{a}^*(i) = 2$. Also, $\alpha_l(\tau)$ and $\exp\{j[2\pi\Delta f(\tau) + \theta_l(\tau)]\}$ are assumed to be constant for one chip ($0\sim T_c$) duration since they are very slowly time-varying in comparison to the chip rate. Similarly, the three noise components of the k-th user for the l-th path are expressed as follows,

$$\begin{aligned}U_{MP_l}(i) &= \frac{1}{2T_c} \sum_{\substack{p=1 \\ p\neq l}}^{L} \int_{\tau_l}^{\tau_l+T_c} \alpha_p(\tau) e^{j[2\pi\Delta f(\tau)+\theta_p(\tau)]} \\ &\quad \times \left(A_0 + \sum_{q=1}^{K} \sqrt{E_c^q} \cdot b^q(\tau-\tau_p) \right. \\ &\quad \left. \times w^q(\tau-\tau_p)\right) \underline{a}(\tau-\tau_p) d\tau \times \underline{a}^*(i) \\ &= \frac{1}{2T_c} \sum_{\substack{p=1 \\ p\neq l}}^{L} \alpha_p(i) e^{j[2\pi\Delta f\cdot i+\theta_p(i)]} \\ &\quad \times \int_0^{T_c} \left(A_0 + \sum_{q=1}^{K} \sqrt{E_c^q} \cdot b^q(t-\tau_e) \right. \\ &\quad \left. \times w^q(t-\tau_e)\right) \underline{a}(t-\tau_e) dt \times \underline{a}^*(i) \\ &= \frac{1}{2} \sum_{\substack{p=1 \\ p\neq l}}^{L} \alpha_p(i) e^{j[2\pi\Delta f\cdot i+\theta_p(i)]} \\ &\quad \times \left(A_0 + \sum_{q=1}^{K} \sqrt{E_c^q} \cdot b^q(i,\tau_e) \right. \\ &\quad \left. \times w^q(i,\tau_e)\right) \underline{a}(i,\tau_e) \cdot \underline{a}^*(i)\end{aligned} \tag{6}$$

$$\begin{aligned}U_{MAI_l}(i) &= \frac{1}{2T_c} \sum_{\substack{q=1 \\ q\neq k}}^{K} \sqrt{E_c^q} \int_{\tau_l}^{\tau_l+T_c} \Big\{ \alpha_l(\tau) \\ &\quad \times e^{j[2\pi\Delta f(\tau)+\theta_l(\tau)]} \left(b^q(\tau-\tau_l)\right. \\ &\quad \left.\times w^q(\tau-\tau_l)\right) \underline{a}(\tau-\tau_l) \Big\} d\tau \times \underline{a}^*(i) \\ &= \frac{1}{2T_c} \sum_{\substack{q=1 \\ q\neq k}}^{K} \Big\{ \sqrt{E_c^q} \alpha_l(i) e^{j[2\pi\Delta f\cdot i+\theta_l(i)]} \\ &\quad \times \int_0^{T_c} b^q(t) w^q(t) \underline{a}(t) dt \Big\} \times \underline{a}^*(i) \\ &= \sum_{\substack{q=1 \\ q\neq k}}^{K} \Big\{ \sqrt{E_c^q} \alpha_l(i) e^{j[2\pi\Delta f\cdot i+\theta_l(i)]} \\ &\quad \times (b^q(i) w^q(i)) \Big\}\end{aligned} \tag{7}$$

$$\begin{aligned}U_{N_l}(i) &= \frac{1}{T_c} \int_{\tau_l}^{\tau_l+T_c} n(\tau) d\tau \times \underline{a}^*(i) = \tilde{n}_l(i) \\ &= \tilde{n}_l^I(i) + j\tilde{n}_l^Q(i)\end{aligned} \tag{8}$$

where $t = \tau - \tau_l$ and $\tau_e = \tau_p - \tau_l$. Then the parameter τ_e is an integer multiple of T_c ($\tau_e = \lambda T_c$, λ is an integer) and the index (i, τ_e) indicates the time of $iT_c + \tau_e$, i.e., $(i+\lambda)T_c$. Since τ_e is greater than one chip, it follows that $\underline{a}(i) \neq \underline{a}^*(i, \tau_e)$, that is, the transmitted PN code's timing is not exactly matched to the timing of the local PN code. We may assume $U_{N_l}(i)$ is a sample value of the AWGN $n(t)$ for the l-th path.

3. Channel Estimation Process

The maximum likelihood optimum channel estimator is shown in Fig. 5. The time variant channel parameters can be estimated by simply averaging over arbitrary number of chips, N_p. When we set N_p to be large,

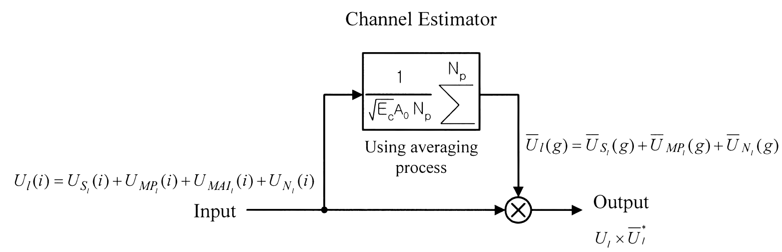

Fig. 5 Channel estimator using maximum likelihood method.

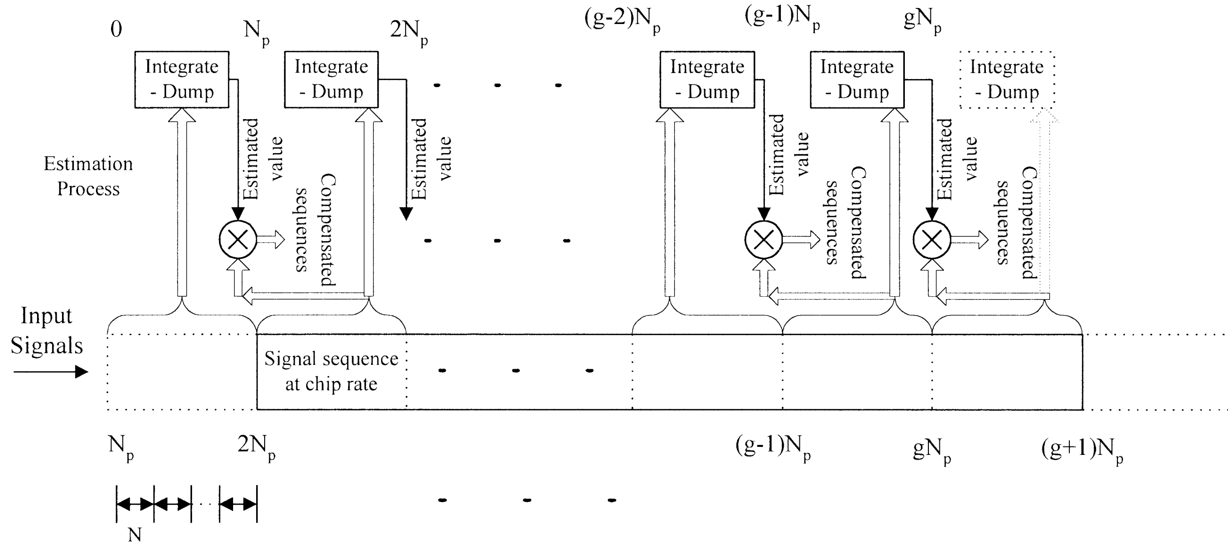

Fig. 6 Conceptual block diagram of the estimated and compensation process for l-th path.

the long period averaging process suppresses the noise influence efficiently. But, the effects of the long averaging intervals lead to systematic errors in the estimated channel coefficients due to the time-variant behavior of the fading channel. Therefore it is necessary to find an optimal N_p considering the channel effects such as SNR, Doppler frequency and residual carrier frequency offset. The various channel effects result in the imperfect receiver phase estimates, which can be represented as the degradation of SNR.

The RAKE receiver with the channel estimator forms the weighted, phase-adjusted, and delay-adjusted sum of the L components. The output of channel estimator amounts to taking the inner product of the received I and Q components with the estimated I and Q component [4],[5],[9],[11]. Therefore, the estimated value of the k-th user is represented as follows:

$$\begin{aligned}\bar{\mathbf{U}} &= \left[\overline{U}_1, \overline{U}_2, \cdots, \overline{U}_l, \cdots, \overline{U}_L\right]^T \\ &= \bar{\mathbf{U}}_S + \bar{\mathbf{U}}_{MP} + \bar{\mathbf{U}}_{MAI} + \bar{\mathbf{U}}_N \qquad (9)\end{aligned}$$

where

$$\begin{aligned}\bar{\mathbf{U}}_S &= [\bar{U}_{S_1}, \bar{U}_{S_2}, \cdots, \bar{U}_{S_l}, \cdots, \bar{U}_{S_L}]^T \\ \bar{\mathbf{U}}_{MP} &= \left[\bar{U}_{MP_1}, \bar{U}_{MP_2}, \cdots, \bar{U}_{MP_l}, \cdots, \bar{U}_{MP_L}\right]^T \\ \bar{\mathbf{U}}_{MAI} &= \left[\bar{U}_{MAI_1}, \bar{U}_{MAI_2}, \cdots, \bar{U}_{MAI_l}, \cdots, \bar{U}_{MAI_L}\right]^T \\ \bar{\mathbf{U}}_N &= \left[\bar{U}_{N_1}, \bar{U}_{N_2}, \cdots, \bar{U}_{N_l}, \cdots, \bar{U}_{N_L}\right]^T\end{aligned}$$

where T indicates the transpose of the matrix and bar means the estimated value.

The time schedule of the channel estimation is shown in Fig. 6. The channel estimator's process operates as follows. First, in order to compensate for the input sequences within $gN_p \sim (g+1)N_p$ chips, the estimated value is obtained by using the input sequences for $(g-1)N_p \sim gN_p$ duration. The time delay between the input sequences for estimation and compensation becomes a maximum of $2N_p$ chips. Second, the estimated value using the input sequences for $(g-1)N_p \sim gN_p$ duration is available only for compensating the input sequences within $gN_p \sim (g+1)N_p$. Therefore, the estimated value is updated every N_p chips. Sequentially, the next estimated value is obtained by using the input sequences for $gN_p \sim (g+1)N_p$ duration, and then the input sequences within $(g+1)N_p \sim (g+2)N_p$ are compensated by using this estimated value. The estimated value of the channel estimator can be written as

$$\overline{U}_l(g) = \frac{1}{\sqrt{E_c}A_oN_p}\sum_{i=(g-1)N_p}^{gN_p-1} U_l(i). \tag{10}$$

We assume that the averaging length N_p is a multiple of the processing gain and the Walsh code's period. Then, from (5)–(7), and (8), the g-th estimated values of the k-th user for l-th path are obtained as

$$\bar{U}_{S_l}(g) = \frac{1}{N_p}\sum_{i=(g-1)N_p}^{gN_p-1}\left[\alpha_l\,(i)\,e^{j[2\pi\Delta f\cdot i+\theta_l(i)]}\right] \tag{11}$$

$$\begin{aligned}\bar{U}_{MP_l}(g) \;=&\; \frac{1}{\sqrt{E_c}A_0N_p}\sum_{i=(g-1)N_p}^{gN_p-1}\sum_{\substack{p=1\\p\neq l}}^{L}\frac{\alpha_p\,(i)}{2}\\ &\times\left(A_0+\sum_{q=1}^{K}\sqrt{E_c^q}\cdot b^q(i,\tau_e)w^q(i,\tau_e)\right)\\ &\times\underline{a}(i,\tau_e)\underline{a}^*(i)e^{j[2\pi\Delta f\cdot i+\theta_p(i)]}\end{aligned} \tag{12}$$

$$\begin{aligned}\bar{U}_{MAI_l}(g) \;=&\; \frac{1}{\sqrt{E_c}A_0N_p}\sum_{i=(g-1)N_p}^{gN_p-1}\sum_{\substack{q=1\\q\neq k}}^{K}\sqrt{E_c^q}\cdot\alpha_p(i)\\ &\times(b^q(i)w^q(i))e^{j[2\pi\Delta f\cdot i+\theta_p(i)]}\end{aligned} \tag{13}$$

$$\bar{U}_{N_l}(g) = \frac{1}{\sqrt{E_c}A_0N_p}\sum_{i=(g-1)N_p}^{gN_p-1}\tilde{n}_l\,(i) \tag{14}$$

At the end of the RAKE receiver, the decision variable of the k-th user for all paths can be represented as follows

$$D = w^k \times \mathbf{U}^T\overline{\mathbf{U}}^* \tag{15}$$

where w is a local Walsh code and the complex conjugation is denoted by an asterisk.

The decision variable of the k-th user at the detector can be expressed as a special case of the general quadratic form [1]

$$D = \sum_{l=1}^{L}\left(w^k\times U_l\bar{U}_l^* + w^k\times U_l^*\bar{U}_l\right) \tag{16}$$

where the local Walsh code $\{w^k\}$ is the same as the transmitted Walsh code sequence of the k-th user. Equation (16) is a special case of an equation in Appendix B of [1] with $A = B = 0$, $C = 1$. For particular values of the j-th bit, the decision variable of the k-th user is

$$\begin{aligned}D(j) \;=&\; \sum_{l=1}^{L}\mathrm{Re}\Bigg[\Bigg\{\sum_{i=gN_p}^{gN_p+N-1} w^k(i)\cdot(U_{S_l}(i)\\ &+U_{MP_l}(i)+U_{MAI_l}(i)+U_{N_l}(i))\Bigg\}\\ &\times\left(\bar{U}_{S_l}^*(g)+\bar{U}_{MP_l}^*(g)+\bar{U}_{MAI_l}^*(g)\right.\\ &\left.+\bar{U}_{N_l}^*(g)\right)\Bigg]\end{aligned} \tag{17}$$

where the summation value for $gN_p \sim gN_p + N - 1$ (chips) duration indicates the j-th data bit.

Since the MAI component is ignored by using the Walsh code (orthogonal spreading code), Eq. (17) can be written as

$$\begin{aligned}D(j) \;=&\; \sum_{l=1}^{L}\mathrm{Re}\Bigg[\Bigg\{\sum_{i=gN_p}^{gN_p+N-1} w^k(i)\cdot(U_{S_l}(i)\\ &+U_{MP_l}(i)+U_{N_l}(i))\Bigg\}\times\left(\bar{U}_{S_l}^*(g)\right.\\ &\left.+\bar{U}_{MP_l}^*(g)+\bar{U}_{N_l}^*(g)\right)\Bigg]\end{aligned} \tag{18}$$

Also, since the MP component is a sum of many independent random variables with zero mean for large processing gain N, we may approximate the MP component by a zero mean Gaussian random variable. From Eqs. (6) and (12), the MP component of the k-th user can be written as follows

$$\begin{aligned}&E\left[\sum_{i=gN_p}^{gN_p+N-1} w^k(i)\cdot U_{MP_l}(i)\right]\\ &\sim \mathrm{N}\left(0, \frac{2}{3}\frac{1}{N}\sum_{\substack{p=1\\p\neq l}}^{L}\mu_p\left(A_0^2E_b+\sum_{q=1}^{K}E_b^q\right)\right)\end{aligned} \tag{19}$$

$$\begin{aligned}&E\left[\bar{U}_{MP_l}(g)\right]\\ &\sim \mathrm{N}\left(0, \frac{2}{3}\frac{1}{N_p}\sum_{\substack{p=1\\p\neq l}}^{L}\mu_p\left(A_0^2E_b+\sum_{q=1}^{K}E_b^q\right)\right)\end{aligned} \tag{20}$$

where μ_p is the p-th average path power, E_b is the average bit power of the Pilot channel, and E_b^q is the average bit power of the q-th user.

4. Performance Analysis

4.1 BER for Binary Phase-Shift Keying (BPSK)

The U_l and $\overline{U}_l$ are a pair of correlated complex-valued gaussian random variables. For the multipath Rayleigh fading channel considered, the L pairs $\{U_l, \overline{U}_l\}$ are mutually statistically independent and identically distributed.

The probability that D is less than zero, denoted here as the probability of error P_b, is

$$P_b \;=\; P(D<0) = \int_{-\infty}^{0} p(D)dD$$

$$= P\left[\sum_{l=1}^{L}\left(wU_{S_l}+wU_{N_l}\right)\left(\bar{U}_{S_l}^{*}+\bar{U}_{N_l}^{*}\right)<0\right] \quad (21)$$

where $p(D)$ is the probability density function of D.

(1) The case of having same power in each paths (similar channel: $\alpha = \alpha_l$ and $\mu = \mu_l$,$\forall l$)

In this case, we assume similar multipah power among L paths. From Appendix B of this paper, we can obtain the BER as follows

$$P_b = \frac{1}{(0.5(1-\mu))^{2L-1}}\sum_{l=0}^{L-1}\begin{pmatrix}2L-1\\ l\end{pmatrix} \times\left(\frac{1+\mu}{1-\mu}\right)^{l} \quad (L>1), \quad (22a)$$

$$P_b = \frac{1}{2}(1-\mu) \quad (L=1), \quad (22b)$$

$$\mu = \sqrt{\left(\mu^{I}_{U_l\overline{U}_l}\right)^2/\{\mu_{U_lU_l}\mu_{\overline{U}_l\overline{U}_l}-\left(\mu^{Q}_{U_l\overline{U}_l}\right)^2\}},$$

where the first and second moments of U_l and $\overline{U}_l$ ($\mu_{U_lU_l}$, $\mu_{\overline{U}_l\overline{U}_l}$, and $\mu_{U_l\overline{U}_l}$) are shown in the next subsection.

(2) The case of having different power in each paths (dissimilar channel : α_l is different, $\forall l$)

In this case, we assume dissimilar multipath power among L paths. In Eq. (21), the probability density function of decision variable D ($p(D)$) is defined as

$$p(D) = \frac{1}{2\pi}\int_{-\infty}^{\infty}\psi_D(j\upsilon)e^{-j\upsilon D}d\upsilon \quad (23)$$

where $\psi_D(j\upsilon)$ is the characteristic function of decision variable D.
The probability of error is

$$P_b = \frac{1}{2\pi}\int_{-\infty}^{0}\int_{-\infty}^{\infty}\psi_D(j\upsilon)e^{-j\upsilon D}d\upsilon dD. \quad (24)$$

In the Rayleigh fading channel, the characteristic function of decision variable D for l-th path from Appendix B of [1] is defined as

$$\begin{aligned}\phi_l(j\upsilon) &= \frac{\upsilon_{1l}\upsilon_{2l}}{(\upsilon+j\upsilon_{1l})(\upsilon-j\upsilon_{2l})} \\ &\quad\times\exp\left[\frac{\upsilon_{1l}\upsilon_{2l}(-\upsilon^2\beta_{1l}+j\upsilon\beta_{2l})}{(\upsilon+j\upsilon_{1l})(\upsilon-j\upsilon_{2l})}\right] \\ &= \frac{\upsilon_{1l}\upsilon_{2l}}{(\upsilon+j\upsilon_{1l})(\upsilon-j\upsilon_{2l})}\end{aligned} \quad (25)$$

where $\beta_{1l} = \beta_{2l} = 0$ from Eq. (A· 14) and (A· 15) in Appendix B of this paper. The characteristic function of decision variable D for L paths is

$$\psi_D(j\upsilon) = \prod_{l=1}^{L}\phi_l(j\upsilon) = \prod_{l=1}^{L}\frac{\upsilon_{1l}\upsilon_{2l}}{(\upsilon+j\upsilon_{1l})(\upsilon-j\upsilon_{2l})} \quad (26)$$

Using the residual theorem, we can obtain the probability of error as follows

$$P_b = (-1)^{L+1}\times\sum_{l=1}^{L}\frac{1}{\upsilon_{2l}}\left[\left(\prod_{k=1}^{L}\frac{\upsilon_{1k}\upsilon_{2k}}{(\upsilon_{2l}+\upsilon_{1k})}\right)\times\left(\prod_{\substack{k=1\\k\neq l}}^{L}\frac{1}{(\upsilon_{2l}-\upsilon_{2k})}\right)\right] \quad (27)$$

where

$$\upsilon_{1l} = \frac{\sqrt{\mu_{U_lU_l}\mu_{\overline{U}_l\overline{U}_l}-\mu^2_{U_l\overline{U}_lQ}}-\mu_{U_l\overline{U}_lI}}{2(\mu_{U_lU_l}\mu_{\overline{U}_l\overline{U}_l}-|\mu_{U_l\overline{U}_l}|^2)}$$

and

$$\upsilon_{2l} = \frac{\sqrt{\mu_{U_lU_l}\mu_{\overline{U}_l\overline{U}_l}-\mu^2_{U_l\overline{U}_lQ}}+\mu_{U_l\overline{U}_lI}}{2(\mu_{U_lU_l}\mu_{\overline{U}_l\overline{U}_l}-|\mu_{U_l\overline{U}_l}|^2)} \quad (28)$$

and the first and second moments of U_l and $\overline{U}_l$ ($\mu_{U_lU_l}$, $\mu_{\overline{U}_l\overline{U}_l}$, and $\mu_{U_l\overline{U}_l}$) are shown in next subsection.

4.2 Computation of the First and Second Moments of U_l and $\overline{U}_l$

Equation (16) depends only on the first and second moments of U_l and $\overline{U}_l$. By using (5), (6), (8), (11), (12), and (14), these parameters of the k-th user are related to the first and second moments of U_l and $\overline{U}_l$ by

$$\begin{aligned}\mu_{U_lU_l} &= 0.5\times E\left[|w^kU_l|^2\right] \\ &= 0.5\times E\left[\left|\left(\sum_{i=gN_p}^{gN_p+N-1}\left\{\sqrt{E_c^k}\alpha_l(i)\times e^{j[2\pi\Delta f(i)+\theta_l(i)]}\right\}+w^k(i)U_{MP_l}(i)+\tilde{n}_l(i)\right)\right|^2\right]\end{aligned} \quad (29)$$

$$\begin{aligned}\mu_{\overline{U}_l\overline{U}_l} &= 0.5\times E\left[\left|\overline{U}_l\right|^2\right] \\ &= 0.5\times E\left[\left|\left\{\sum_{i=(g-1)N_p}^{gN_p-1}\left(\frac{\sqrt{E_c^k}}{N_p}\alpha_l(i)\times e^{j[2\pi\Delta f(i)+\theta_l(i)]}\right)+\frac{1}{\sqrt{E_c}A_0N_p}\tilde{n}_l(i)\right\}+\overline{U}_{MP_l}(g)\right|^2\right]\end{aligned} \quad (30)$$

$$\mu_{U_l\overline{U}_l} = 0.5\times E\left[w^kU_l\overline{U}_l^{*}\right]$$

$$
\begin{aligned}
&= 0.5 \times E\left[\left(\frac{N}{N_p}\sum_{i=gN_p}^{(g+1)N_p-1}\left\{\sqrt{E_c^k}\alpha_l(i)\right.\right.\right.\\
&\quad \left.\times e^{j[2\pi\Delta f(i)+\theta_l(i)]}\right\} + \left.\frac{1}{\sqrt{E_c}A_0N_p}\tilde{n}_l(i)\right)\\
&\quad \times\left(\frac{1}{N_p}\sum_{i=(g-1)N_p}^{gN_p-1}\left\{\alpha_l(i)e^{[j2\pi\Delta f(i)+\theta_l(i)]}\right\}\right.\\
&\quad \left.\left.+\frac{1}{\sqrt{E_c}A_0N_p}\tilde{n}_l(i)\right)\right] \qquad (31)
\end{aligned}
$$

The first- and second-order statistics are obtained from the various random variables of the received signal (α, θ, and U_N) and deterministic parameter (Δf). Note that the Rayleigh random variables ($\{\alpha_l\}$, $\{\theta_1\}$) are independent of the noise random variable [10].

Statistically, the random variables only depend on the delay between the estimated value and the input signal from Appendix A of this paper. Therefore, the statistics can be represented as

$$
\begin{aligned}
\mu_{U_lU_l} &= 0.5 \times NE_c^kE\left[\alpha_l^2(t)\right]\\
&+E_c^k\sum_{n=1}^{N}(N-n)\cos(2\pi\Delta f\cdot n)E\left[\alpha_l(t)\right.\\
&\left.\times\ \alpha_l(t-n)\cos\left(\theta_l(t)-\theta_l(t-n)\right)\right]\\
&+E_c^k\sum_{n=1}^{N}(N-n)\sin(2\pi\Delta f\cdot n)E\left[\alpha_l(t)\right.\\
&\left.\times\ \alpha_l(t-n)\sin\left(\theta_l(t)-\theta_l(t-n)\right)\right]\\
&+\frac{2}{3N}\sum_{\substack{p=1\\p\neq l}}^{L}\mu_p^k\left(A_o^2E_b+E_b^k\right)\\
&+0.5\times N\times N_o \qquad (32)
\end{aligned}
$$

where the notation t indicates an arbitrary time index. Similarly, $\mu_{\overline{U}_l\overline{U}_l}$ and $\mu_{U_l\overline{U}_l}$ can be written as follows:

$$
\begin{aligned}
\mu_{\overline{U}_l\overline{U}_l} &= 0.5\times\frac{1}{N_p}E\left[\alpha_l^2(t)\right]\\
&+\frac{1}{N_p^2}\sum_{n=1}^{N_p}(N_p-n)\cos(2\pi\Delta f\cdot n)E\left[\alpha_l(t)\right.\\
&\left.\times\ \alpha_l(t-n)\cos\left(\theta_l(t)-\theta_l(t-n)\right)\right]\\
&+\frac{1}{N_p^2}\sum_{n=1}^{N_p}(N_p-n)\sin(2\pi\Delta f\cdot n)E\left[\alpha_l(t)\right.\\
&\left.\times\ \alpha_l(t-n)\sin\left(\theta_l(t)-\theta_l(t-n)\right)\right]\\
&+\frac{2}{3N_p}\sum_{\substack{p=1\\p\neq l}}^{L}\mu_p^k\left(A_o^2E_b+E_b^k\right)\\
&+0.5\times\frac{1}{E_cA_o^2N_p}N_o \qquad (33)
\end{aligned}
$$

$$
\mu_{U_l\overline{U}_l} = 0.5\times\left(\mu^I_{U_l\overline{U}_l}+j\mu^Q_{U_l\overline{U}_l}\right) \qquad (34)
$$

Table 1 The parameters of the channel environment.

PARAMETERS	VALUES
Chip rate	1.2288 MHz
Walsh code's period M	64
PN code's period	32767(2^{15}-1)
Processing gain N	128
Pilot power	1
Data power	0.78125
Multipath profile for 3 paths	Similar : 1/3, 1/3, 1/3 Dissimilar : 0.5 , 0.3 , 0.2 Dissimilar : 0.8 , 0.15 , 0.05
Carrier frequency	1.8 GHz

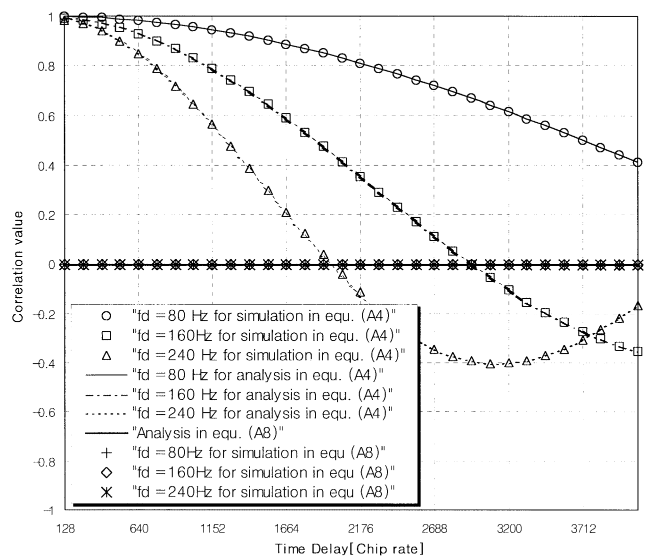

Fig. 7 Correlation function of the Rayleigh fading $E[\alpha_l(t)\alpha_l(t-\tau)\cos\{\theta_l(t)-\theta_l(t-\tau)\}]$ and $E[\alpha_l(t)\alpha_l(t-\tau)\sin\{\theta_l(t)-\theta_l(t-\tau)\}]$.

where

$$
\begin{aligned}
\mu^I_{U_l\overline{U}_l} &= \frac{N\sqrt{E_c^k}}{N_p^2}\sum_{n=N_p}^{2N_p-1}\sum_{m=1}^{N_p-1}\{\cos(2\pi\Delta f(n-m))\\
&\times E\left[\alpha_l(t-n)\alpha_l(t-m)\right.\\
&\left.\times\ \cos\left(\theta_l(t-n)-\theta_l(t-m)\right)\right]\\
&+\sin(2\pi\Delta f(n-m))E\left[\alpha_l(t-n)\right.\\
&\left.\times\ \alpha_l(t-m)\sin\left(\theta_l(t-n)-\theta_l(t-m)\right)\right]
\end{aligned} \qquad (35)
$$

$$
\begin{aligned}
\mu^Q_{U_l\overline{U}_l} &= \frac{N\sqrt{E_c^k}}{N_p^2}\sum_{n=N_p}^{2N_p-1}\sum_{m=1}^{N_p-1}\{\sin(2\pi\Delta f(n-m))\\
&\times E\left[\alpha_l(t-n)\alpha_l(t-m)\right.\\
&\left.\times\ \cos\left(\theta_l(t-n)-\theta_l(t-m)\right)\right]\\
&+\cos(2\pi\Delta f(n-m))E\left[\alpha_l(t-n)\right.\\
&\left.\times\ \alpha_l(t-m)\sin\left(\theta_l(t-n)-\theta_l(t-m)\right)\right]
\end{aligned} \qquad (36)
$$

where the index n indicates the input sequence

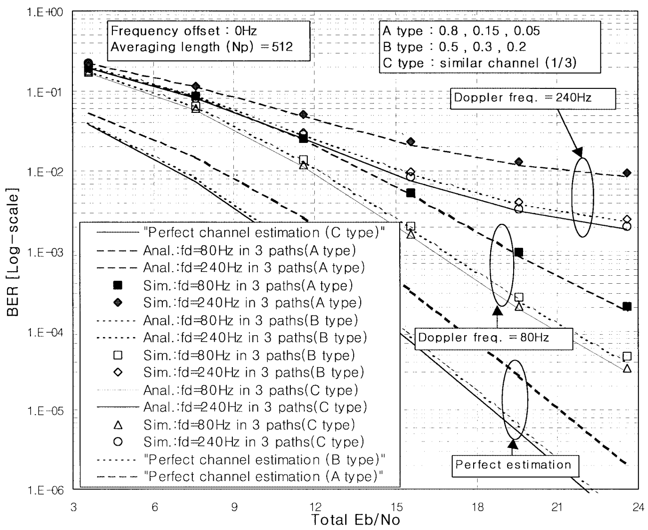

Fig. 8 BER vs. total E_b/N_o for 3 paths without interference.

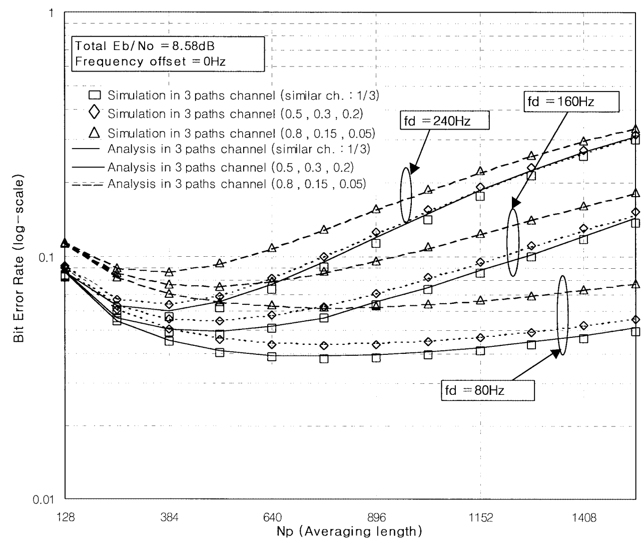

Fig. 9 BER vs. averaging length for various Doppler frequency spreads in 3 paths environment without interference.

for the channel compensation process (complex multiplier) and the index m indicates the input sequence for the channel estimation process. The correlation functions of Rayleigh fading channel ($E\left[\alpha_l(t)\alpha_l(t-\tau)\cos(\theta_l(t)-\theta_l(t-\tau)\right]$ and $E\left[\alpha_l(t)\alpha_l(t-\tau)\sin(\theta_l(t)-\theta_l(t-\tau)\right]$) are respectively shown in the Appendix A of this paper.

5. Numerical and Simulation Results

The channel parameters used in this paper are shown in Table 1. Figure 7 shows computer simulation for the expected values of Rayleigh fading, $E[\alpha_l(t)\alpha_l(t-\tau)\cos(\theta_l(t)-\theta_l(t-\tau)]$ and $E[\alpha_l(t)\alpha_l(t-\tau)\sin(\theta_l(t)-\theta_l(t-\tau)]$. In this figure, we verify that the computer simulation is exactly same as the analytic results derived in Appendix A of this paper. The simulator of Doppler shift effect (time selective fading) is modeled by using the spectral filter to shape random signals in the frequency domain. The total E_b/N_o for BPSK data modulation is defined as

$$\text{Total}\frac{E_b}{N_o} = (\text{traffic channel data power} + \text{pilot channel power}) \times \frac{T}{T_c} \times \frac{E_c}{N_o}$$

Figure 8 shows the BER curves for imperfect channel estimation as well as perfect channel estimation. And the BER curves are obtained for $N_p = 512$, frequency offset $= 0$ Hz, and various Doppler frequencies ($f_d = 80$ and 240 Hz). But the multipath interference (MPI) is not considered. The difference in the required total E_b/N_o between perfect estimation and imperfect estimation is approximately 4 dB for $f_d = 80$ Hz, when the BER is 10^{-2} for 3 paths. And, the difference in the required total E_b/N_o between perfect estimation and imperfect estimation is approximately 10 dB for $f_d = 240$ Hz, when the BER is 10^{-2} for 3 paths. Also, as the main path's power is increased and the other path's powers are decreased, the channel environment of the three paths is close to the channel environment of the one path. Therefore, in different channel environments, we can obtain the best performance in the case of the similar channel and the worst performance in the case of the A type dissimilar channel (0.8, 0.15, 0.05). Additionally, we can verify that the chip-based simulation results for BER vs. total E_b/N_o are exactly the same as the numerical results derived in this paper.

When the multipath interference (MPI) is not considered, Fig. 9 shows the BER curve versus the averaging length N_p for various Doppler frequencies from slow fading (80 Hz) to fast fading (240 Hz). From Fig. 9, we can see that the optimal averaging length for a minimum BER depends on the Doppler frequency. But, the optimal averaging length is not changed for different multipath channel environment. Also, we confirm that the optimal N_p decreases as the Doppler frequency increases. Even when the optimal N_p is used, BER degradation increases as the Doppler frequency increases. Also, the numerical results are the same as the simulation results. Therefore, we can obtain the optimal averaging length for a minimum BER with respect to the channel parameters.

Figure 10 shows the BER performance versus carrier frequency offset. Figure 11 shows numerical results of the BER performance for residual carrier frequency offset and Doppler frequency spread. The results are obtained when there is no interference (MPI and other users). It is seen that as the carrier frequency offset is increased, the BER performance is declined remarkably. Even if the speed of a mobile is limited within 100 km/hr, the influence of residual carrier frequency

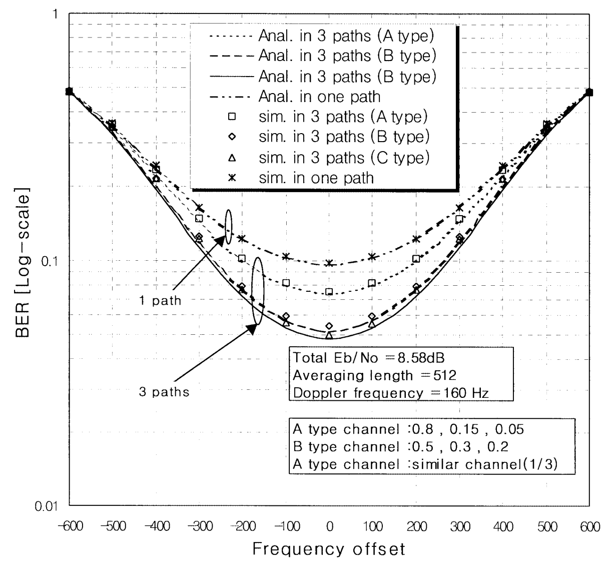

Fig. 10 BER vs. carrier frequency offset for various Doppler frequency spreads without interference.

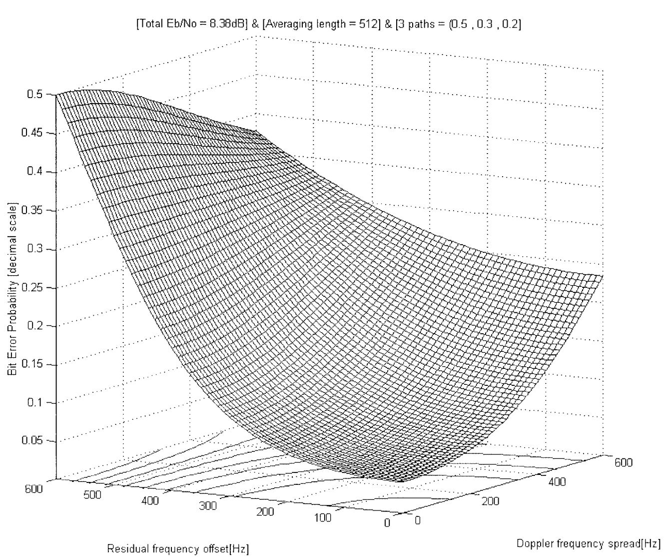

Fig. 11 BER vs. residual carrier frequency offset and Doppler frequency spread in 3 paths channel environment without interference.

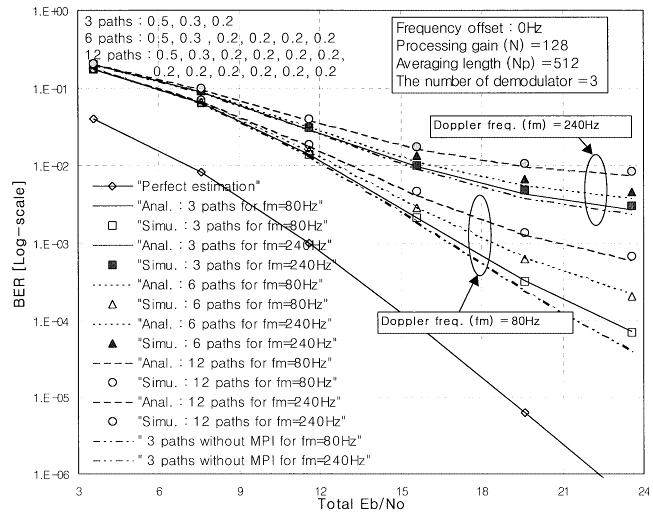

Fig. 12 BER vs. total E_b/N_o for multiple paths with multipath interference and no other users.

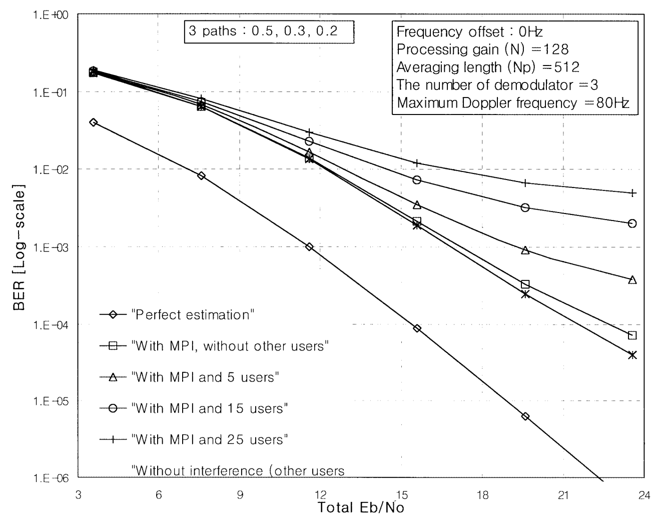

Fig. 13 BER vs. total E_b/N_o for 3 paths with multipath interference and other users.

offset on the degradation of BER is more serious than that of the Doppler frequency spread.

Figure 12 shows the BER curves for the total E_b/N_o without other users. Three fingers (demodulators) are used and each curve is obtained for the number of the paths (3, 6, and 12) and maximum Doppler frequency. The performance degradation increases relative to the no multipath interference as the total E_b/N_o is increased. Consequently, the effect of the error floor is shown due to the increase of the resolvable paths and maximum Doppler frequency.

Figure 13 shows the BER curves for the total E_b/N_o with MPI (multipath interference) and other users. But the number of paths is fixed at 3 paths and the average energy of each user is assumed to be equal. The BER performance is degraded as the interference is increased. From the Gaussian approximation of MPI and other users, it is noted that the effect of the MPI and other users are dominant relative to AWGN especially as the number of user or resolvable paths are increased. Also, compared to Fig. 12, effect of other users increased the degradationfurther.

6. Conclusion

A closed-form BER solution for DS-CDMA RAKE receiver with imperfect channel estimation has not been available previously in the literatures. In this paper, the performance of DS-CDMA receiver considering imperfect channel estimation was presented in a closed form

BER equation under various channel environments such as Doppler shift, SNR and carrier frequency offset.

By the analysis and simulation, we evaluated the performance of DS-CDMA RAKE receiver in the forward link and presented the optimal channel estimation parameters under various channel environments. In addition, the results indicate that BER degradations, relative to AWGN including the interference (MAI and MPI), are sensitive to Doppler frequency and residual carrier frequency offset. This fact is much more useful in practice than the ideal BER performance presented in previous works. Ultimately, the system SNR is determined by the statistical functions of the Rayleigh fading and the residual frequency offset.

These contributions are expected to help in predicting the system's performance and in optimizing the parameters setting for the channel estimation. We believe the presented analysis in this paper can be easily extended to evaluate and design the next generation wideband CDMA system such as QPSK-modulated BPSK-spreading scheme or QPSK-modulated QPSK-spreading scheme.

Although only single-cell environment is investigated in this paper primarily for analytical simplicity, effect of other-cell interference in multicell environment is interesting and can not be ignored in practice. Modeling and evaluation of other-cell interference is complicated, however, and should be addressed as a sequel to this paper in the future.

References

[1] J.G. Proakis, Digital Communications, McGraw-Hill, 1995.
[2] M. Kavehrad and B. Ramamurthi, "Direct-sequence spread spectrum with DPSK modulation and diversity for indoor, wireless communication," IEEE Trans. Comm., vol.COM-35, no.2, pp.224–236, Feb. 1987.
[3] H. Ochsner, "Direct-sequence spread-spectrum receiver for communication on frequency-selective fading channels," IEEE J. Select. Areas Commun., vol.SAC-5, pp.188–193, Feb. 1987.
[4] C. Sandeep and S.C. Gupta, "Performance of an adaptive multipath diversity receiver in a frequency selective Rayleigh fading channel," in Proc. of IEEE Veh. Technol. Conf. (VTC'88), Philadelphia, PA, pp.351–357, June 1988.
[5] U. Fawer, "A coherent spread-spectrum diversity-receiver with AFC for multipath fading channels," IEEE Trans. Comm., vol.42, no.2/3/4, pp.1300–1311, Feb./March/April 1994.
[6] Q.T. Zhang, "Probability of error for equal-gain combiners over Rayleigh channels: some closed-form solutions," IEEE Trans. Comm., vol.45, no.3, pp.270–273, March 1997.
[7] T. Eng and L.B. Milstein, "Partially coherent DS-SS performance in frequency selective multipath fading," IEEE Trans. Comm., vol.45, no.1, pp.110–118, Jan. 1997.
[8] M. Benthin and K.-D. Kammeyer, "Influence of channel estimation on the performance of a coherent DS-CDMA system," IEEE Trans. VT, vol.46, no.2, pp.262–267, May 1997.
[9] A.J. Viterbi, Principles of Spread Spectrum Communication, Addison-Wesley Publishing Company, 1995.
[10] W.C. Jakes, Microwave Mobile Communications, Wiley-Interscience Publication, 1974.
[11] T.S. Rappaport, Wireless Communications: Principles and Practice, IEEE PRESS, 1996.
[12] I.S. Gradshteyn and I.M. Ryzhik, Table of Integrals, Series, and Products, Academic Press, 1980.
[13] R.L. Peterson, R.E. Ziemer, and D.E. Borth, Introduction to Spread Spectrum Communications, Prentice-Hall, 1995.
[14] I. Korn, "M-ary CPFSK-DPD with L-diversity maximum ratio combining in rician fast-fading channels," IEEE Trans. VT, vol.45, no.4, pp.613–621, May 1996.

Appendix A: The Expected Values of the Correlation Functions

In this Appendix, we calculate the expected values of the correlation functions $E\,[\alpha_l(t)\alpha_l(t-\tau)\,\cos(\theta_l(t)\,-\theta_l(t-\tau)]$ and $E\,[\alpha_l(t)\alpha_l(t-\tau)\,\sin(\theta_l(t)\,-\theta_l(t-\tau)]$.

Let $\alpha_l(t)$ be r_1, $\alpha_l(t-\tau)$ be r_2, and $\theta_l(t)-\theta_l(t-\tau)$ be ϕ. By using the joint pdf of Rayleigh fading [10], the expected value of $E\,[r_1r_2\cos\phi]$ is

$$\begin{aligned} E\,[r_1r_2\cos\phi] &= 2\pi\int_0^\infty\int_0^\infty\int_{-\pi}^{\pi}\{r_1r_2\cos\phi \\ &\quad\times P\,(r_1,r_2,\phi)\}\,d\phi dr_1dr_2 \\ &= \int_0^\infty\int_0^\infty\int_{-\pi}^{\pi}\{r_1r_2\cos\phi \\ &\quad\times\frac{r_1r_2}{2\pi\mu^2\,(1-\lambda^2)} \\ &\quad\times\exp\left[-\frac{r_1^2+r_2^2}{2\mu\,(1-\lambda^2)}\right] \\ &\quad\times\exp\left[\frac{\lambda r_1r_2\cos\phi}{\mu\,(1-\lambda^2)}\right]\Bigg\}\,d\phi dr_1dr_2 \end{aligned} \tag{A$\cdot$1}$$

where, $\lambda = J_0\,(\omega_m\tau)(\;\omega_m\tau$: maximum Doppler frequency) and $2\mu = E[(\alpha^I)^2] = E[(\alpha^Q)^2]$ is the mean power of Rayleigh fading.

From the Table of integrals [12], the triple integral in (A$\cdot$1) can be reduced to a form

$$\begin{aligned} E\,[r_1r_2\cos\phi] &= \frac{1}{\mu^2(1-\lambda^2)}\int_0^\infty\int_0^\infty\Big\{r_1^2r_2^2 \\ &\quad\times\exp\left(-\frac{r_1^2+r_2^2}{2\mu(1-\lambda^2)}\right) \\ &\quad\times I_1\left(\frac{r_1r_2\lambda}{\mu(1-\lambda^2)}\right)\Bigg\}\,dr_1dr_2 \end{aligned} \tag{A$\cdot$2}$$

where $I_n(x)$ is the n-th order modified Bessel function of the first kind. From the Table of integrals [12], the double integral in (A$\cdot$2) can be reduced to a form

$$\begin{aligned} E\,[r_1r_2\cos\phi] &= \frac{\lambda}{\mu}\int_0^\infty r_2^3\exp\left(-\frac{r_2^2}{2\mu}\right) \\ &\quad\times\;{}_1F_1\left(0;2;-\frac{\lambda^2r_2^2}{2\mu(1-\lambda^2)}\right)dr_2 \end{aligned}$$

(A·3)

where, ${}_1F_1(a;b;z)$ is the confluent hypergeometric function [12]. Finally, the expected value of $E[r_1r_2\cos\phi]$ is arranged in a compact form as

$$E[r_1r_2\cos\phi] = \begin{cases} 4\mu\lambda(1-\lambda^2)^2 \times \sum_{n=0}^{\infty} \frac{(2)_n}{n!}\lambda^{2n}, & (|\lambda|<1) \\ 1, & (|\lambda|=1) \end{cases} \tag{A·4}$$

where $(a)_n$ is the shifted factorial function, i.e.,$(a)_n = a\cdot(a+1)\cdot(a+2)\cdots$.

In the same manner as in (A·1), the expected values of $E[\alpha_l(t)\alpha_l(t-\tau)\sin(\theta_l(t)-\theta_l(t-\tau)]$ is

$$\begin{aligned} E[r_1r_2\sin\phi] &= 2\pi\int_0^{\infty}\int_0^{\infty}\int_{-\pi}^{\pi}\{r_1r_2\sin\phi \\ &\quad \times P(r_1,r_2,\phi)\}\,d\phi dr_1dr_2 \\ &= \int_0^{\infty}\int_0^{\infty}\int_{-\pi}^{\pi} r_1r_2\sin\phi \\ &\quad \times \frac{r_1r_2}{2\pi\mu^2(1-\lambda^2)} \cdot \\ &\quad \times \exp\left[-\frac{r_1^2+r_2^2}{2\mu(1-\lambda^2)}\right] \\ &\quad \times \exp\left[\frac{\lambda r_1r_2\cos\phi}{\mu(1-\lambda^2)}\right] d\phi dr_1dr_2 \end{aligned} \tag{A·5}$$

where the integral of sine term is evaluated as,

$$\begin{aligned} \int_{-\pi}^{\pi}\sin\phi\cdot e^{z\cos\phi}d\phi &= \int_0^{\pi} -\sin\phi\cdot e^{-z\cos\phi}d\phi \\ &\quad + \int_0^{\pi}\sin\phi\cdot e^{z\cos\phi}d\phi \\ &= \frac{2}{z}\sinh(-z) + \frac{2}{z}\sinh(z) \\ &= 0 \end{aligned} \tag{A·6}$$

$$\int_0^{\pi}\sin x\cdot e^{a\cos x}dx = \frac{2}{a}\sinh(a) \tag{A·7}$$

Finally, the expected value of $E[r_1r_2\sin\phi]$ is

$$E[r_1r_2\sin\phi] = 0. \tag{A·8}$$

Appendix B: The BER Performance for the Case of Equal Power

In this Appendix, we derive the BER performance for the case of equal power in each paths. Starting from Eq. (14), which is a special case of an equation in Appendix B of [1] with $A=B=0$, $C=1$, the probability in (17) can be derived to be

$$\begin{aligned} P_b &= Q_1(a,b) - I_0(ab)\exp\left[-\frac{1}{2}(a^2+b^2)\right] \\ &\quad + \frac{I_0(ab)\exp\left[-\frac{1}{2}(a^2+b^2)\right]}{(1+\upsilon_2/\upsilon_1)^{2L-1}}\sum_{l=0}^{L-1}\left\{\binom{2L-1}{l}\right. \\ &\quad \times \left.\left(\frac{\upsilon_2}{\upsilon_1}\right)^l\right\} + \frac{\exp\left[-\frac{1}{2}(a^2+b^2)\right]}{(1+\upsilon_2/\upsilon_1)^{2L-1}} \\ &\quad \times \sum_{n=1}^{L-1} I_n(ab)\sum_{l=0}^{L-1-n}\binom{2L-1}{l} \\ &\quad \times \left[\left(\frac{b}{a}\right)^n\left(\frac{\upsilon_2}{\upsilon_1}\right)^l - \left(\frac{a}{b}\right)^n\left(\frac{\upsilon_2}{\upsilon_1}\right)^{2L-1-l}\right], \\ &\qquad (L>1) \end{aligned} \tag{A·9}$$

$$\begin{aligned} P_b &= Q_1(a,b) - \frac{\upsilon_2/\upsilon_1}{1+\upsilon_2/\upsilon_1}I_0(ab) \\ &\quad \times \exp\left[-\frac{1}{2}(a^2+b^2)\right], \qquad (L=1) \end{aligned} \tag{A·10}$$

Here $I_n(x)$ is the n-th order modified Bessel function of the first kind and

$$Q(a,b) = \begin{cases} e^{-0.5(a^2+b^2)}\sum_{n=0}^{\infty}\left(\frac{a}{b}\right)^n I_n(a,b), & (a<b) \\ 1 - e^{-0.5(a^2+b^2)}\sum_{n=0}^{\infty}\left(\frac{a}{b}\right)^n I_n(a,b), & (b<a) \end{cases} \tag{A·11}$$

where

$$\begin{aligned} a &= \left[\frac{2\upsilon_1^2\upsilon_2(\beta_1\upsilon_2-\beta_2)}{(\upsilon_1+\upsilon_2)^2}\right]^{1/2}, \\ b &= \left[\frac{2\upsilon\upsilon_2^2(\beta_1\upsilon_1+\beta_2)}{(\upsilon_1+\upsilon_2)^2}\right]^{1/2}, \end{aligned} \tag{A·12}$$

and

$$\begin{aligned} \upsilon_1 &= \frac{\sqrt{\mu_{U_lU_l}\mu_{\overline{U}_l\overline{U}_l} - \mu^2_{U_l\overline{U}_lQ}} - \mu_{U_l\overline{U}_lI}}{2(\mu_{U_lU_l}\mu_{\overline{U}_l\overline{U}_l} - |\mu_{U_l\overline{U}_l}|^2)}, \\ \upsilon_2 &= \frac{\sqrt{\mu_{U_lU_l}\mu_{\overline{U}_l\overline{U}_l} - \mu^2_{U_l\overline{U}_lQ}} + \mu_{U_l\overline{U}_lI}}{2(\mu_{U_lU_l}\mu_{\overline{U}_l\overline{U}_l} - |\mu_{U_l\overline{U}_l}|^2)}. \end{aligned} \tag{A·13}$$

For the Rayleigh channel [10],[14] , we have

$$\begin{aligned} \beta_1 &= 2(|E[U_l]|^2\mu_{\overline{U}_l\overline{U}_l} + |E[\overline{U}_l]|^2\mu_{U_lU_l} \\ &\quad - E[U_l]^*E[\overline{U}_l]\mu_{U_l\overline{U}_l} - E[U_l]E[\overline{U}_l]^*\mu^*_{U_l\overline{U}_l}) \\ &= 0 \end{aligned} \tag{A·14}$$

$$\beta_2 = E[U_l]^* E[\overline{U}_l] + E[U_l] E[\overline{U}_l]^* = 0 \qquad \text{(A· 15)}$$

where $E[U_l] = E[\overline{U}_l] = 0$ [10]. Therefore, in Eq. (A· 12), we can set $a = b = 0$.

Since $Q(0,0) = 1$, $I_0(0) = 1$, $I_n(0) = 0$ for $n \neq 0$ we obtain from Eq. (A· 9) and (A· 10)

$$P_b = \begin{cases} \frac{1}{(0.5(1-\mu))^{2L-1}} \sum_{l=0}^{L-1} \begin{pmatrix} 2L-1 \\ l \end{pmatrix} \left(\frac{1+\mu}{1-\mu}\right)^l & (L > 1) \\ \frac{1}{2}(1-\mu) & (L = 1) \end{cases} \qquad \text{(A· 16)}$$

where

$$\mu = \sqrt{\frac{\left(\mu^I_{U_l\overline{U}_l}\right)^2}{\mu_{U_lU_l}\mu_{\overline{U}_l\overline{U}_l} - \left(\mu^Q_{U_l\overline{U}_l}\right)^2}}. \qquad \text{(A· 17)}$$

and where the first and second moments of U_l and $\overline{U}_l$ ($\mu_{U_lU_l}$, $\mu_{\overline{U}_l\overline{U}_l}$, and $\mu_{U_l\overline{U}_l}$) are shown in Sect. 4.2.

Seokjun Ko received the B.S.E.E. and M.S.E.E. degrees from Sung Kyun Kwan University, Korea in 1996 and 1998, respectively. Since 1998, he has been working towards the Ph.D. degree in the Department of Electrical and Computer Engineering from Sung Kyun Kwan University. His research interests are mobile communications (CDMA) and modem technology with associated digital signal processing.

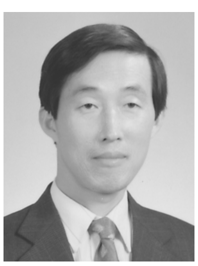

Hyungjin Choi received the B.S.E. E. degree from the Seoul National University, Korea in 1974, the M.S.E.E. degree from the Korea Advanced Institute of Science, Korea in 1976, and the Ph.D. degree in Electrical Engineering (communications major) from the University of Southern California, Los Angeles in 1982. From 1976 to 1979 he worked for the Central Research Lab. of the Gold Star Co., Seoul, Korea, as a research engineer. From 1983 to 1989, he worked for the Lincom Corp., Los Angeles, California. Since March 1989, he has been a faculty member with the Department of Electronics Engineering(now, Department of Electrical and Computer Engineering), Sung Kyun Kwan University, Korea and currently holds the rank of Professor. His main field of interests includes mobile radio engineering, satellite communications, communication system engineering, and digital modulation/demodulation with associated signal processing and synchronization.